Available online at www.sciencedirect.com

ScienceDirect

Advances in Space Research 69 (2022) 1281–1300

ADVANCES IN SPACE RESEARCH (a COSPAR publication)

www.elsevier.com/locate/asr

Spread-F characteristics over Tucumán near the southern anomaly crest in South America during the descending phase of solar cycle 24

Gilda de Lourdes González *

Facultad de Ingeniería, Universidad del Norte "Santo Tomás de Aquino", Tucumán, Argentina
Facultad de Ciencias Exactas y Tecnología, Universidad Nacional de Tucumán, Tucumán, Argentina

Received 23 May 2021; received in revised form 3 November 2021; accepted 10 November 2021
Available online 17 November 2021

Abstract

Ionospheric F-region irregularities can acutely affect navigation and communication systems. To develop predictive capabilities on their occurrence, it is key to understand their variabilities in a wide range of time scales. Previous studies at low latitudes in South America have been performed mostly in the eastern region. However, there are still few reports on the spread-F over Argentina owing to a lack of ionosonde data. This work presents the analysis of the spread-F (range spread-F and frequency spread-F) and plasma bubble occurrence characteristics near the southern crest of the Equatorial Ionization Anomaly in Argentina (Tucumán, 26.8°S, 65.2°W; magnetic latitude 15.5°S). We used ionosonde and Global Positioning System (GPS) data from November 2014 to December 2019 for different solar and geomagnetic conditions. The data show that spread-F and plasma bubble occurrence rates peak in local summer and are minimum in equinox and winter, respectively. There is a negative correlation between each type of spread-F and solar activity, whereas the opposite happens for plasma bubbles. Geomagnetic activity suppresses the generation of spread-F in equinox and summer and enhances it in winter. Plasma bubble occurrence is higher during disturbed days than during quiet days, but under medium solar activity, summer months register more plasma bubbles in quiet conditions. Range spread-F observed in winter under low solar activity is not associated with plasma bubbles originated at the magnetic equator. These results contribute to the knowledge necessary to improve the prediction of the spatial and temporal distribution of the night-time ionospheric irregularities.

Keywords: Low latitude Ionosphere; Equatorial spread-F; Plasma bubbles; Ionospheric irregularities

1. Introduction

Ionospheric irregularities are regions in the ionosphere with electron density noticeably different from the background, caused by plasma instability processes. Their scale sizes range from centimetres to hundreds of kilometres, and the duration can vary between minutes and several hours. The ionospheric irregularities have been an important subject of investigation since they were discovered (Booker and Wells, 1938), mainly due to their adverse effects on communication and navigation systems. To mitigate this negative influence is necessary to advance in the understanding of this ionospheric phenomenon and improve our prediction capabilities.

If irregularities are present in the F region above an ionosonde, a backscatter signature called spread-F may be seen in ionograms. These are due to the presence of km-scale irregularities. Spread-F can be classified into bottom-side spread F, irregularities confined to the bottom-side F region, and top-side spread-F, associated with the generation of equatorial plasma bubbles (EPBs) (Valladares et al., 1983; Woodman and La Hoz, 1976).

* Corresponding author at: Facultad de Ingeniería, Universidad del Norte "Santo Tomás de Aquino", 9 de Julio 165, T4000 San Miguel de Tucumán, Argentina.
E-mail address: gilda.gonzalez@unsta.edu.ar.

https://doi.org/10.1016/j.asr.2021.11.009
0273-1177/

EPBs are large-scale depletions of F region electron density. They are generated at the equator at the bottom-side of the F layer and grow non-linearly into the topside. As EPBs vertically develop, they propagate to low latitudes aligned to the geomagnetic field lines, by effects of diffusion, gravity and pressure gradient (Balan et al., 2018). The effect of broadening in frequency is known as frequency spread-F (FSF) and in height, range spread-F (RSF), a mixed pattern can be also observed, and it is referred as mixed spread-F (MSF), traces are broadened in both range and frequency (Piggott and Rawer, 1978).

A Total Electron Content (TEC) depletion is a sudden reduction of TEC followed by a recovery to a level near the value preceding the depletion (Valladares et al., 2004). Many researchers have pointed out that these are a manifestation of EPBs (DasGupta et al., 1983; Tsunoda and Towle, 1979; Weber et al., 1996; Shetti et al., 2019). Global Positioning System (GPS) signal delays are proportional to the TEC along the satellite-receiver line of sight. Thus, GPS data can derive the TEC (Çepni et al., 2013; Dashora and Pandey, 2005). Because of the magnetic latitude of Tucumán, RSF and TEC depletions may be associated with plasma bubbles extending up to the top side of the layer. FSF is related to smaller-scale decaying irregularities near the F region peak (Abdu et al., 1981b). It is important to note that a plasma bubble may not contain small-scale irregularities during the late evening time. So, during this period, it is possible to observe TEC depletions but not spread-F.

At equatorial and low latitude regions, the generation of ionospheric irregularities can be attributed to the gravitational Rayleigh-Taylor instability mechanism (Balsley et al., 1972; Dungey, 1956; Calvert, 1963). Their initiation is related to the upward E × B drift and the uplifting of the F-layer. These electric fields could be generated by the ionospheric dynamo or imposed from the magnetosphere. A condition for the generation of irregularities is that the E layer conductivity cannot short out the driving electric field. At sunset, the E layer at equatorial regions disappears due to chemical recombination and the pre-reversal enhancement in the eastward electric field (PRE) raises the F layer rapidly. This creates favourable conditions for the occurrence of irregularities. Besides the Rayleigh-Taylor instability, a seeding process acting at the bottom side of the F layer is required to initiate the perturbations. Some possible seeding sources are gravity waves from the lower atmosphere, medium-scale travelling ionospheric disturbances (MSTIDs), large-scale wave structures (LSWSs) and the solar terminator (Röttger, 1973; Taori et al., 2015; Tsunoda et al., 2011).

Moreover, Tsunoda (1985) proposed that the seasonal/-longitudinal distribution of the irregularities occurrence rate depends on the magnetic declination angle, i.e., in the geometry between the geomagnetic field line and the terminator line. When the sunset terminator aligns with the magnetic meridian, sunset is simultaneous at conjugate E regions and the eastward polarization electric field is maximum, this enhances the vertical ExB drift. The low-density plasma of the lower heights rises to the topside ionosphere as plasma bubbles. Its latitudinal extension is related to the apex height (equatorial crossing altitude) of the bubble and, therefore, to the strength of the PRE (Anderson and Haerendel, 1979; Mendillo and Tyler, 1983). The plasma density irregularities depend on local time, season, latitude and longitude, and solar and geomagnetic activities, in addition to their day-to-day variability (Abdu et al., 1985; Pietrella et al., 2017; Tsunoda 1985; Yizengaw and Groves 2018). Therefore, the analysis of their characteristics in different locations and periods is essential.

The effects of solar and geomagnetic activities on spread-F vary with latitude and longitude. Previous studies investigated the relationship between the spread-F occurrence and the geomagnetic and solar conditions at low latitudes using geophysical indices (Kp, Dst, F10.7 and Sn) (Aquino and Sreeja 2013; Bowman and Mortimer 2003; Kotulak et al., 2020). Whalen (2003) suggested that plasma bubble occurrence decrease with the Kp index during equinox and December solstice in South America. Becker-Guedes et al.(2004) discussed the spread-F occurrence during geomagnetic storms at three stations in the eastward Brazilian sector. They concluded that during the low equatorial plasma bubble occurrence season and transition season, the geomagnetic activity helped in the generation of plasma bubbles and inhibited it during the high plasma bubble occurrence season. Abdu et al. (1998) examined data from three stations in South America, including Tucumán, for four intervals: 1980–81 (F10.7 = 161.5) and 1988–89 (F10.7 = 173.8) representing solar maximum conditions, and 1984–85/1986–87 (F10.7 = 83.7/73.6) representing solar minimum conditions. Their results showed that there was an increase in the spread-F occurrence rate with solar flux. Also, the spread-F occurrence was maximum in the summer months at Tucumán.

Several researchers have studied the occurrence of F region irregularities over the equatorial ionization anomaly (EIA) crest region in different longitudinal sectors, using data from a wide variety of diagnostic techniques: ionosonde, ground-based Global Navigation Satellite System (GNSS), optical imaging techniques, radar observations and in situ satellite measurements (Cueva et al., 2013; Li et al., 2020; Muella et al., 2010; Pietrella et al., 2017; Reinisch et al., 2004; Sahai et al., 1994; Timoçin et al., 2020; Weber et al., 1978). They found that multiple factors control the occurrence of irregularities such as the pre-reversal enhancement (PRE), seed perturbations, density gradient at the F layer bottom side, the *trans*-equatorial winds and the altitude of the F layer (Farley et al., 1970; Fejer et al., 1999; Yokoyama et al., 2004).

In the Brazilian region, earlier works showed a high plasma bubble occurrence rate during the December solstice and a low occurrence during the June solstice (Abdu et al., 1998; Sahai et al., 1994). Chum et al. (2016) examined the spread-F behaviour over Tucumán and Taiwan

in 2014 based on measurements by continuous Doppler sounding. They observed the highest occurrence rate from September to March in Tucumán, and around equinoxes in Taiwan. Alfonsi et al. (2013) performed spread-F statistics of occurrence at Tucumán during October 2010–September 2011. They reported that the occurrence of all types of spread-F was maximum in local summer and minimum in local winter.

Although many researchers have discussed the characteristics of ionospheric irregularities at low latitudes, some aspects still need to be further investigated to better understand the spatial and temporal variability of spread-F and plasma bubbles. Therefore, the analysis of large data sets for various solar and magnetic conditions is useful. In South America, most studies have been done for the eastern Brazilian region, characterized by a magnetic declination angle of $\sim$ 20°W. Whereas the magnetic declination angle in Tucumán is $\sim$ 7°W. Albeit some works have examined the spread-F occurrence in Tucumán (Abdu et al., 1998; Alfonsi et al., 2013; Cabrera et al., 2010; Pezzopane et al., 2013), we considered herein a longer period of analysis: November 2014 to December 2019. This work aims to contribute to the knowledge of the characteristics of spread-F and plasma bubbles during different local times, seasons, solar and geomagnetic conditions at the southern crest of the EIA. For this purpose, we analysed the occurrence percentages of RSF, FSF and TEC depletion using ionosonde and GPS data sets at Tucumán during the descending phase of solar cycle 24.

2. Methodology

We studied the irregularities occurrence at Tucumán, Argentina (26.8°S, 65.2°W; magnetic latitude 15.5°S), a station near the southern crest of the EIA. We analysed 1038 days of ionosonde data and 1310 days of GPS data. The period considered was November 2014 to December 2019, the descending phase of Solar Cycle 24, as it is indicated by the sunspot number Sn (http://www.sidc.be/silso/-dayssnplot). During 2019 the monthly mean sunspot number was between 0.4 and 9.9 and the yearly mean sunspot number was 3.6. From November 2014 to December 2015, the monthly mean Sn was between 54.5 and 112.9. The yearly mean Sn for 2015 was 69.8 and the average Sn for Nov-Dec 2014 was 113.6.

We manually examined the ionograms recorded by the Vertical Incidence Pulsed Ionospheric Radar (VIPIR) by following the Manual of Ionogram Scaling (Wakaiet al., 1987) and the U.R.S.I Handbook (Piggott and Rawer 1978). The VIPIR operates between 1.5 and 25 MHz with a sounding repetition rate of 5 min (Bullett 2008). The field-of-view covers 60° of the sky. The data availability is shown in Fig. 1 and the ionograms can be downloaded from the website of the Low Latitude Ionospheric Sensor Network (LISN) (http://lisn.igp.gob.pe). We analysed the occurrence rate (equation (1)) of two types of spread-F: RSF and FSF (Fig. 2) during 18:00–06:00 LT (UT = L T + 4) and their mean duration (equation (2)).

$$\text{Occurrence rate } (\%) = \frac{\text{Number of days with spreadF at time T in a month}}{\text{Number of days with ionograms at time T in the month}} \times 100 \quad (1)$$

$$\text{SpreadF duration} = \frac{\text{Total spreadF duration}}{\text{Total number of spreadF events}} \quad (2)$$

To examine the seasonal behaviour, we grouped the data into March equinox (March and April), June solstice (May, June, July, and August), September equinox (September and October), and December solstice (November, December, January, and February). We considered F10.7 and Ap index to identify the solar and geomagnetic conditions. F10.7 $\leq$ 100, 100 $<$ F10.7 $<$ 180, and F10.7 $\geq$ 180 represent low, medium, and high solar activity, respectively (Abdu et al., 2003). Ap $<$ 12 indicates geomagnetic quiet days and Ap $\geq$ 12 disturbed days (Fig. 3). F10.7 is provided by Dominion Radio Astrophysical Observatory and Natural Resources Canada (https://www.spaceweather.gc.ca/solarflux/sx-en.php) and Ap index is produced by Geomagnetic Observatory Niemegk, GFZ German Research Centre for Geosciences (https://www.gfz-potsdam.de/en/home/).

To compare the behaviour of RSF and plasma bubbles, we considered TEC depletions greater than 5 TECu (1 TECu = 10^{16} electron/m^2) to be associated with plasma bubbles (Magdaleno et al., 2012). Hence, we used ground-based GPS-TEC data at Tucumán to calculate the plasma bubbles occurrence rate (number of days with TEC depletions greater than 5 TECu, divided by the total number of days analysed).

The Receiver INdependent EXchange (RINEX) files are available at the LISN website, unfortunately, there are no measurements for September–December 2017 and April–December 2019. The vertical TEC (VTEC) was calculated from GPS observables got from RINEX files using the analysis code developed by Seemala and Valladares (2011). We derived TEC every 10 s. The effects of multipath were reduced by applying a 30° elevation mask. Therefore, TEC measurements cover $\sim$ 120° of the sky.

3. Results

3.1. Monthly and seasonal variations of the spread-F occurrence

During the period analysed, the most common type of spread-F was RSF (65.3%). According to the occurrence rate (Figs. 4–8), RSF began at 20–22 LT and lasted until 5–6 LT. The peak occurrence rate was usually around 23–1 LT, whereas for May-August the maximum came up later. FSF generally arose after midnight and peaked

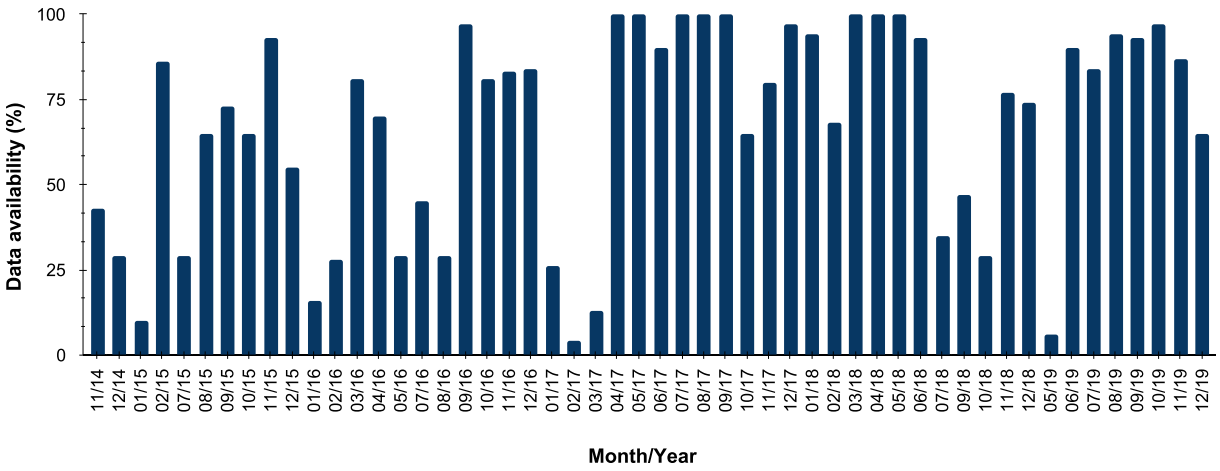

Fig. 1. Ionogram data availability per month in Tucumán station from November 2014 to December 2019.

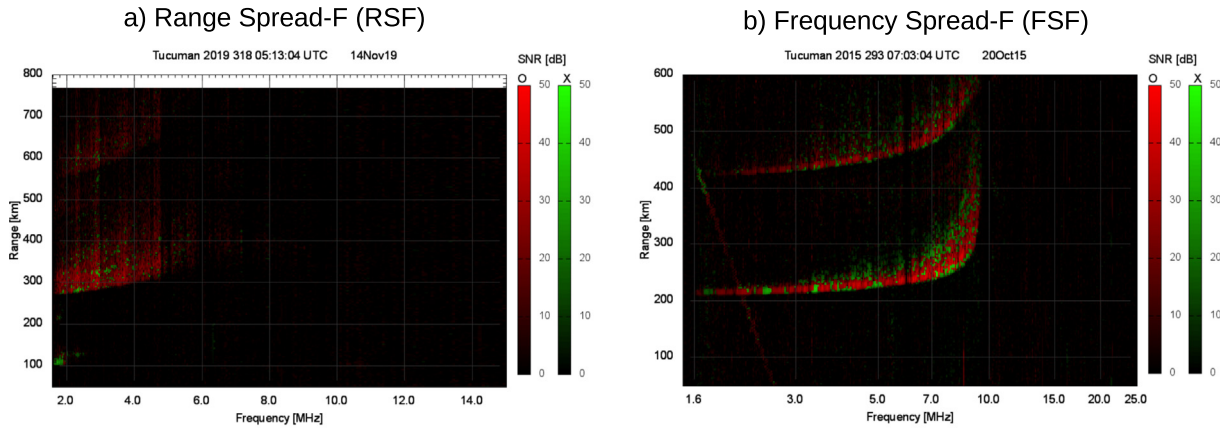

Fig. 2. Ionograms showing examples of (a) range spread-F (RSF) and (b) frequency spread-F (FSF).

around 3 LT. September equinox registered the lowest spread-F (RSF and FSF) occurrence (61%) and December solstice the highest (84%). Fig. 9 depicts the seasonal total spread-F (both RSF and FSF) occurrence rate for each year. December solstice presented the highest occurrence every year (from 62% in 2015 to 95% in 2017) except in 2018 when the maximum was in June solstice (90%). The season with the lowest occurrence percentage (12%) was June solstice, 2015. It is worth mentioning that 2018 showed a high occurrence of spread-F in all seasons, between 70% in September equinox and 90% in June solstice.

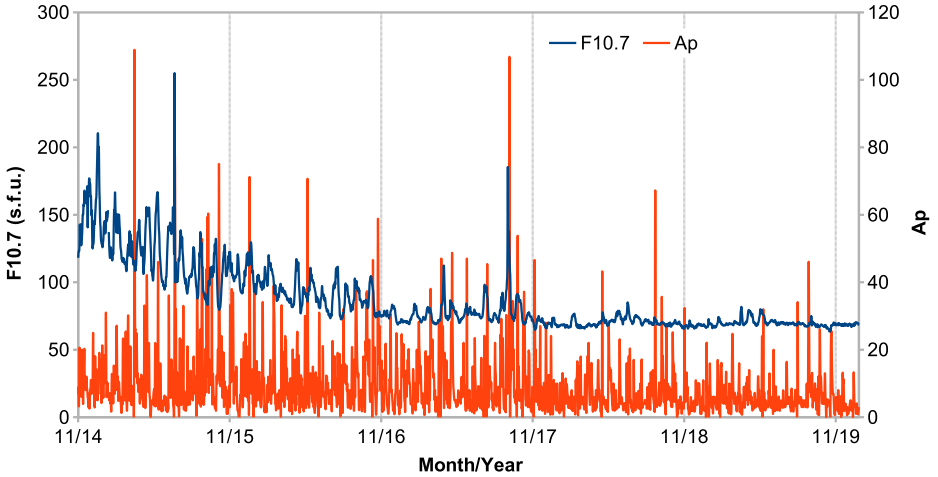

Fig. 3. Daily F10.7 and Ap index from November 2014 to December 2019.

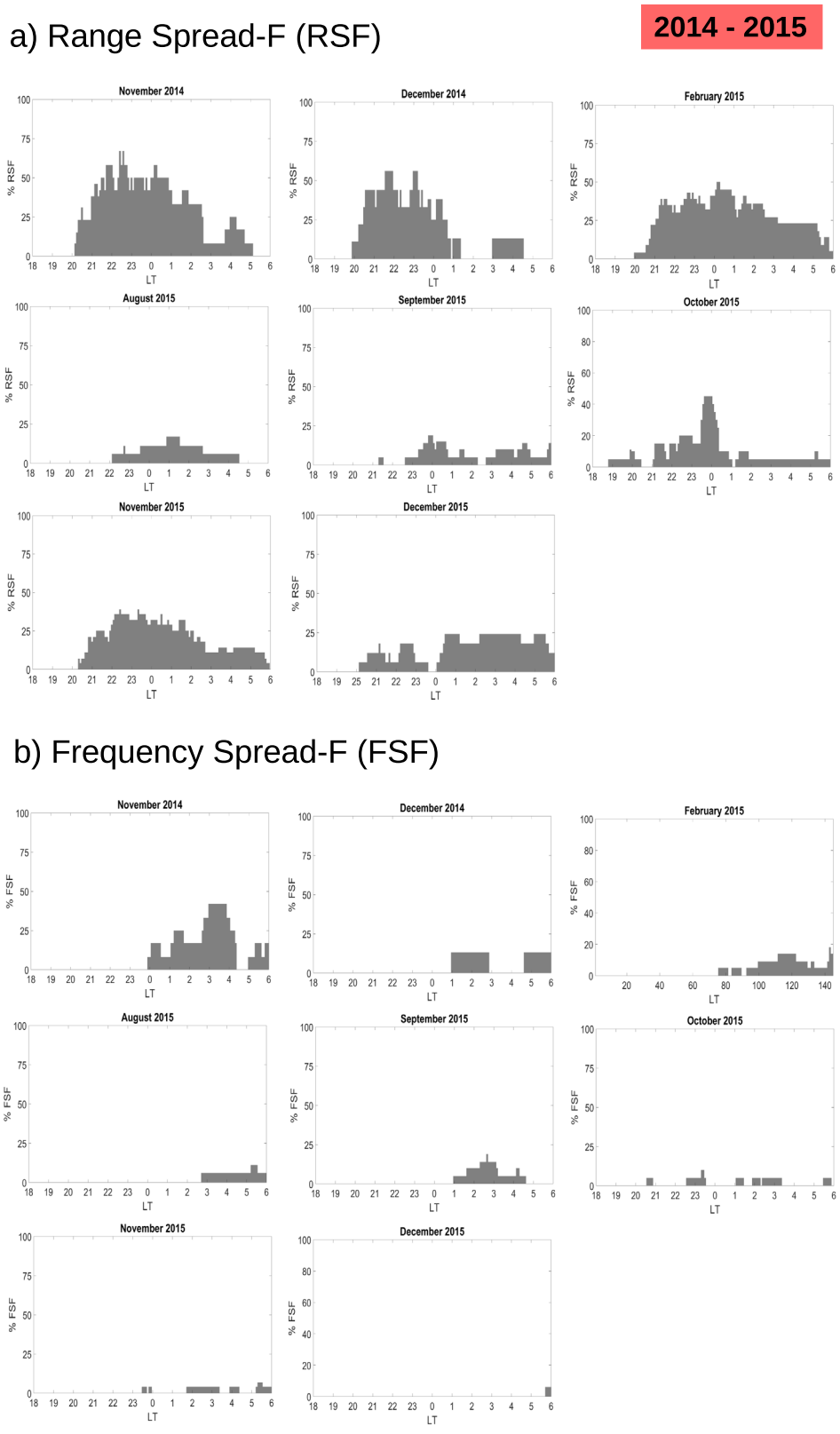

Fig. 4. Occurrence rate of (a) range spread- F (RSF) and (b) frequency spread-F (FSF) over Tucumán station during November 2014 – December 2015.

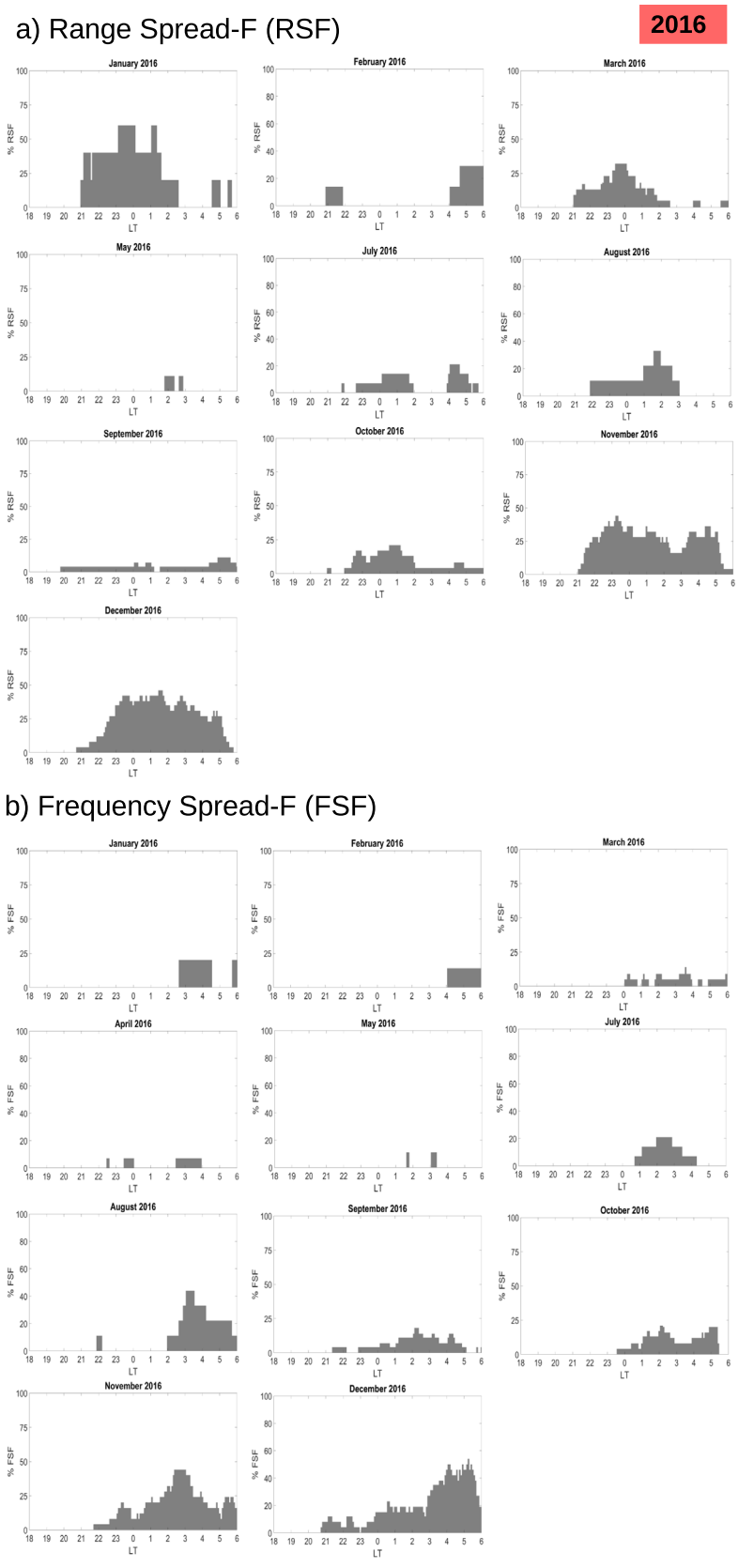

Fig. 5. Occurrence rate of (a) range spread- F (RSF) and (b) frequency spread-F (FSF) over Tucumán station during 2016.

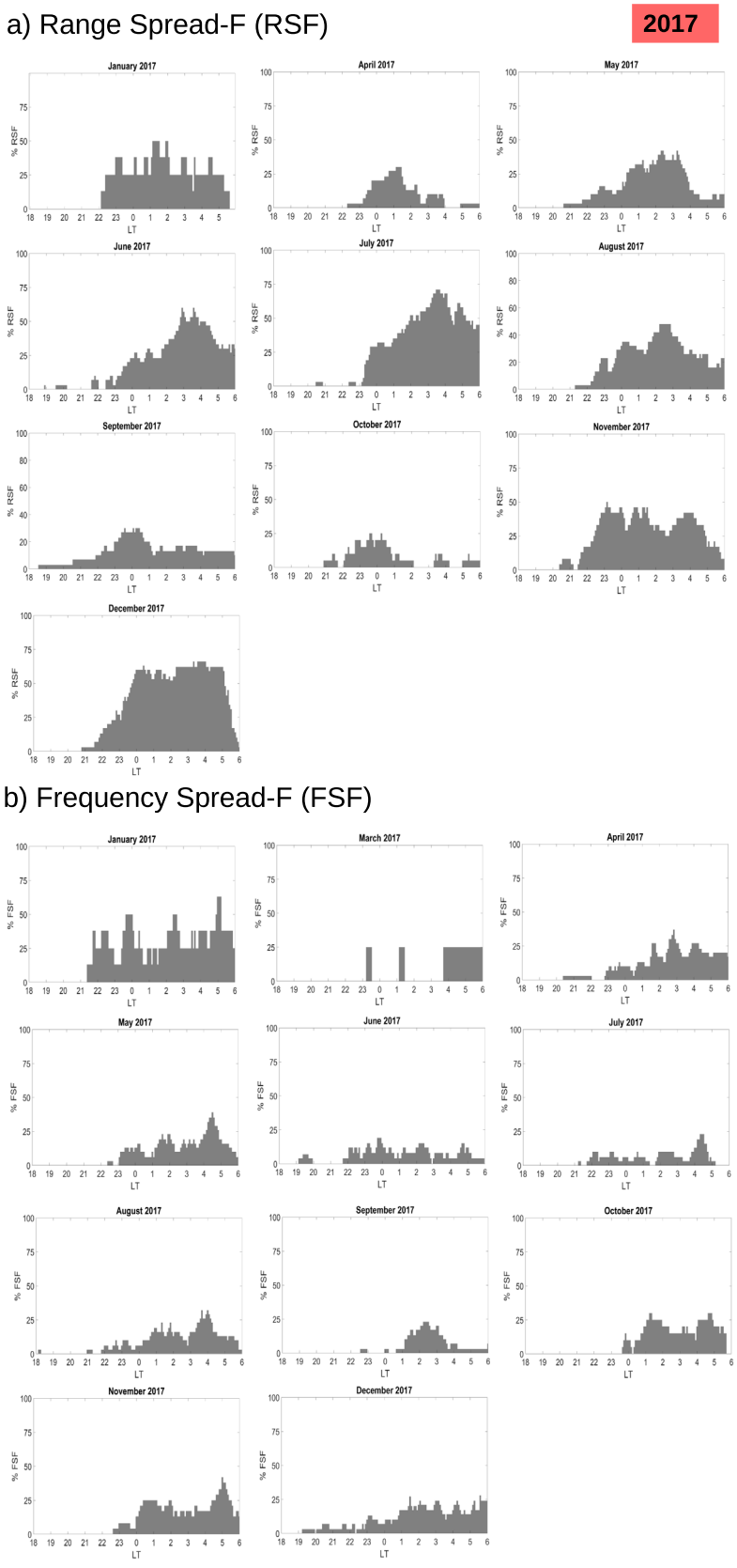

Fig. 6. Occurrence rate of (a) range spread-F (RSF) and (b) frequency spread-F (FSF) over Tucumán station during 2017.

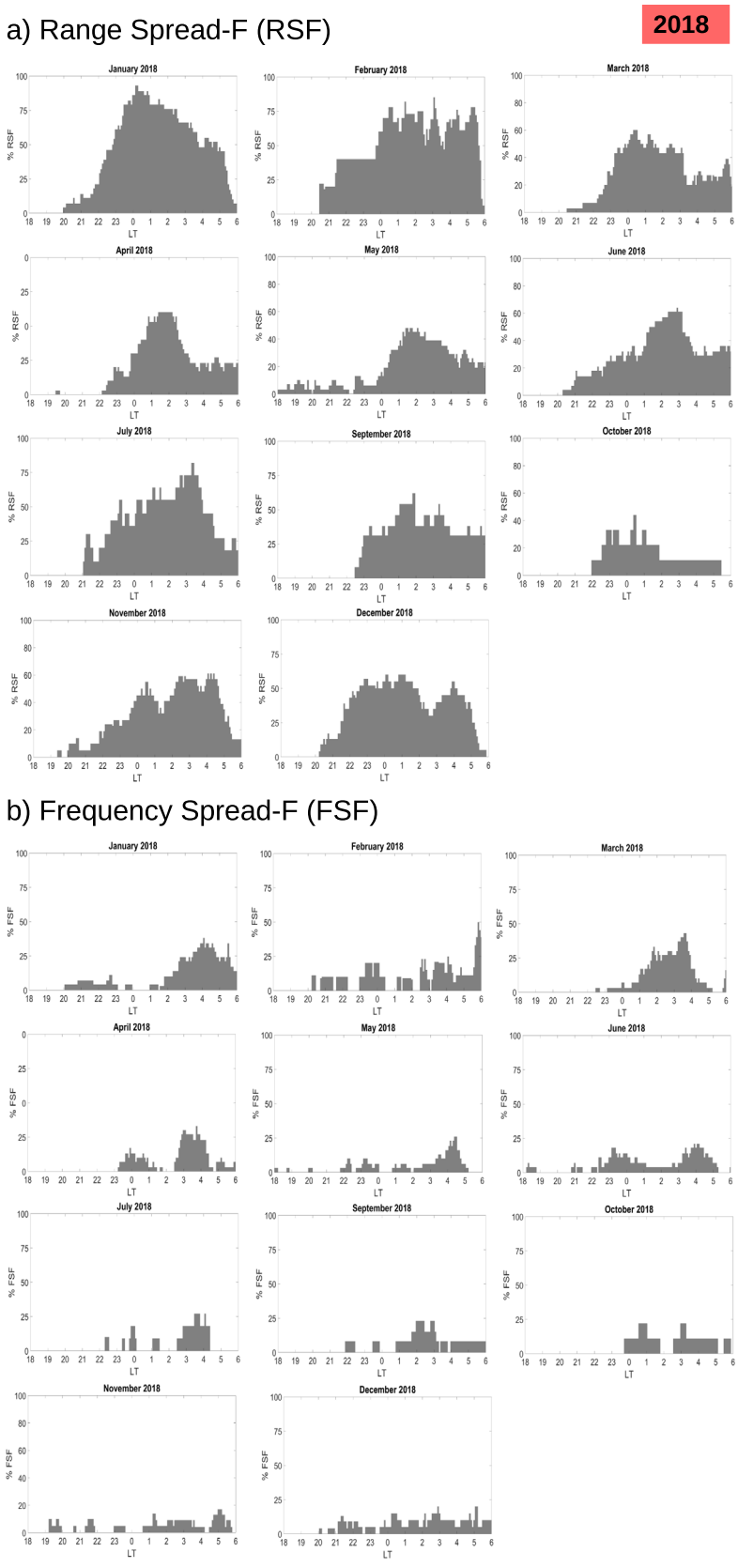

Fig. 7. Occurrence rate of (a) range spread- F (RSF) and (b) frequency spread-F (FSF) over Tucumán station during 2018.

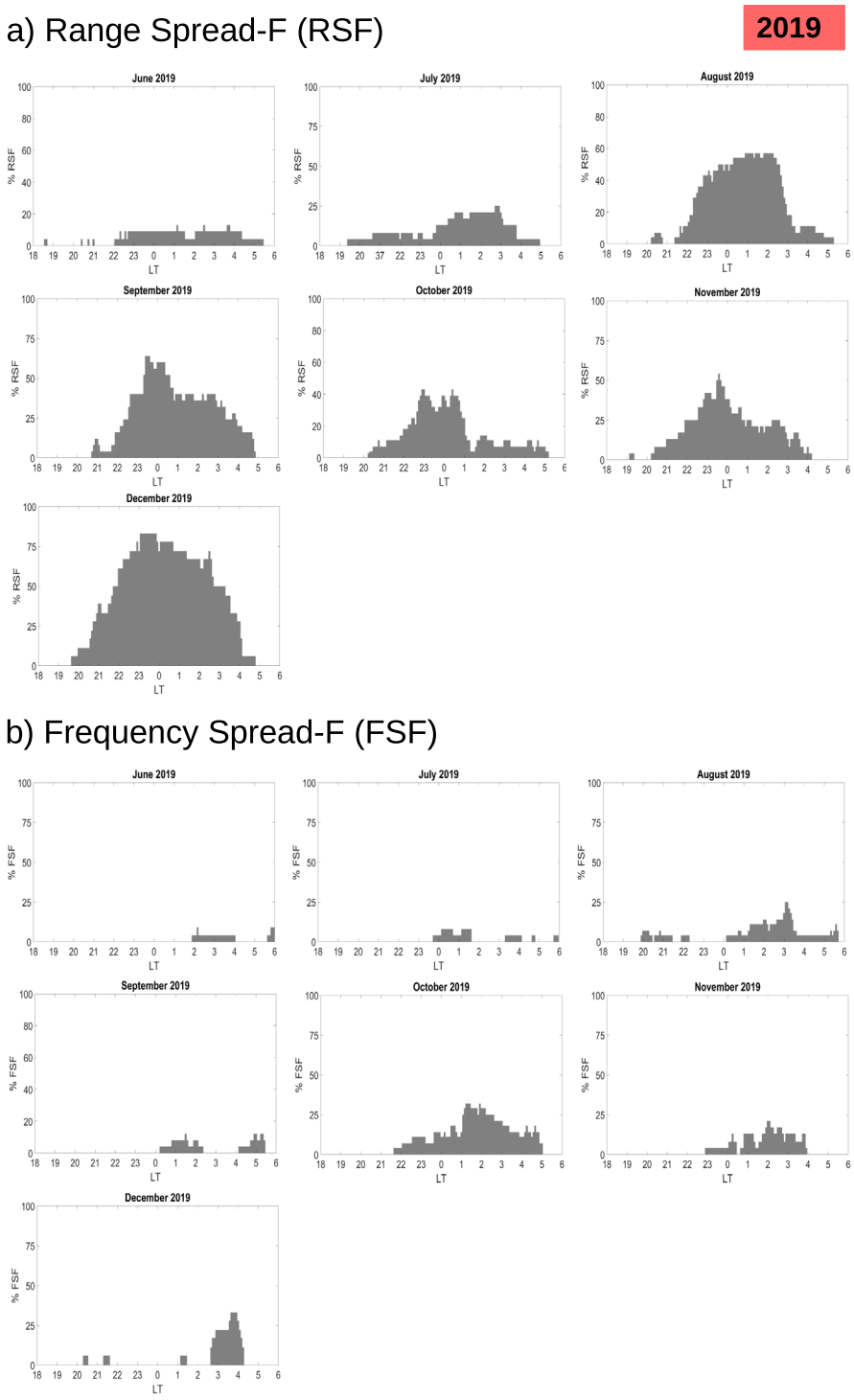

Fig. 8. Occurrence rate of (a) range spread- F (RSF) and (b) frequency spread-F (FSF) over Tucumán station during 2019.

Tables 1, 2 and Fig. 10 show the seasonal occurrence of RSF and FSF for the years considered in this work. The data show that RSF occurrence was highest in December solstice 2017, whereas FSF was maximum in December solstice 2016, and both showed their lowest occurrence in June solstice 2015. RSF was more frequent than the other types of spread-F in all seasons except between September 2016 and April 2017 when FSF occurrence was higher. The mean RSF duration tended to increase during the period studied, whereas the opposite happened for the FSF (Fig. 11). RSF lasted around ~ 1–3 h and FSF ~ 0.5–2 h. During years of low solar activity—2017, 2018 and 2019— RSF duration showed maximum values (2.1 – 2.5 h) in the December solstice.

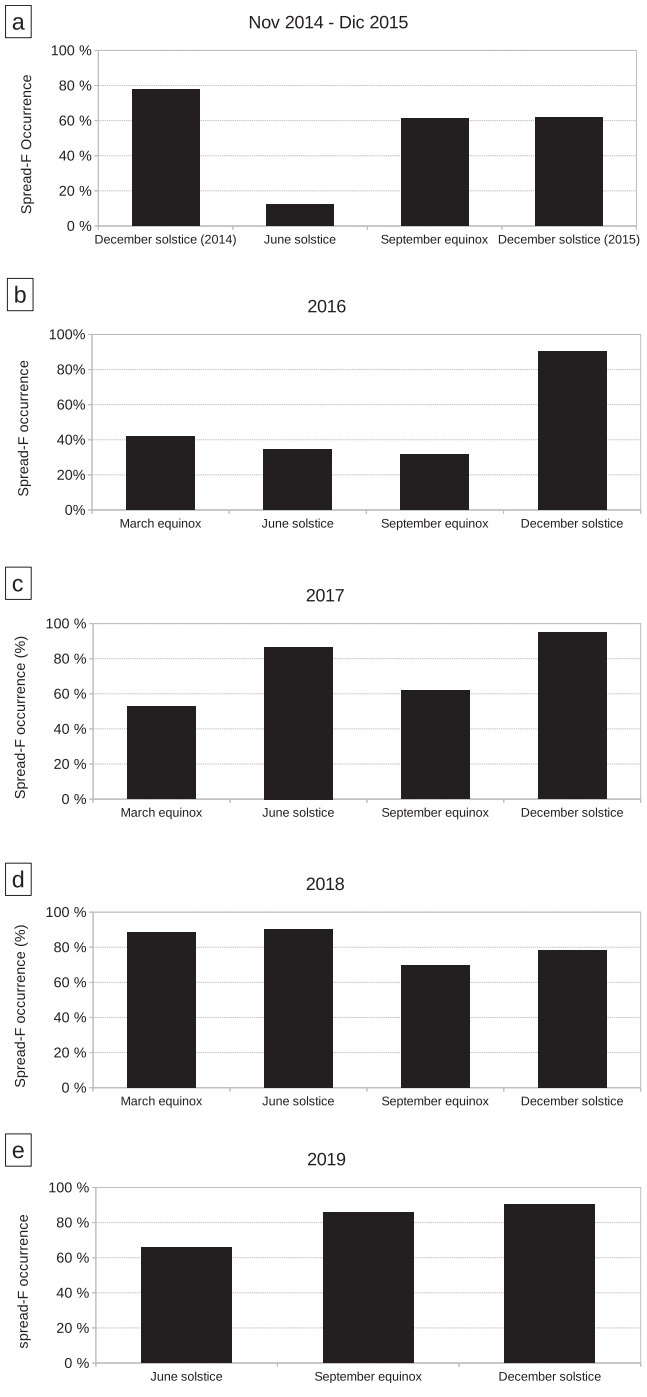

Fig. 9. Seasonal occurrence rate of spread-F (both RSF and FSF) in Tucumán during November 2014-December 2019. This is the percentage of days with at least one spread F event daily in a season.

3.2. Spread-F occurrence rate during different solar and geomagnetic conditions

Fig. 12 shows that spread-F occurrence increased between 2016 (53.3%) when the mean F10.7 was 88.7 sfu (sfu is solar flux unit: 10^{-22} Wm^{-2} Hz^{-1}) and 2018 (84.5%) when the mean F10.7 was 69.9 sfu, and decreased in 2019 (78.2%) when the mean F10.7 was 77.3 sfu. Regarding the different types of spread-F, RSF and FSF occurrence rate generally increased when the F10.7 index decreased, especially between 2015 and 2018. Similarly, RSF and FSF increased when the mean Ap index decreased between 2015 and 2019. These observations do not allow us to draw a conclusion on the solar flux dependence of spread-F because of the small range of values of F10.7. To get a better description of the variability of the spread-F occurrence with solar activity, we would need data for the entire solar cycle (Abdu et al., 1998). Unfortunately, the VIPIR ionosonde was installed in 2014, so we do not have ionograms for the ascending phase of solar cycle 24.

For the period examined here, there were seven days with high solar activity (F10.7 $\geq$ 180), and just one had ionosonde data available (4/9/17, F10.7 = 186). So, in this analysis, we only considered days with low (F10.7 $\leq$ 100) and medium (100 $<$ F10.7 $\langle$180) solar activity levels. Fig. 13 shows the occurrence rates of RSF and FSF under low and medium solar activity in Tucumán. RSF and FSF occurrence rates decreased with solar activity in all seasons, except for the September equinox when RSF was higher during medium solar activity than during low solar activity (58.1% vs 51.3%). At the March equinox, RSF was only present during low solar activity, 58.3%. The FSF occurrence rate was 33.3% during medium solar activity and 53.5% during low solar activity. At the June solstice, the RSF occurrence was 5.6% during medium solar activity and 66.8% during low solar activity. The FSF was absent during medium solar activity, and its occurrence was 49.2% during low solar activity. At the September equinox, the FSF occurrence rate was 29% during medium solar activity and 36.1% during low solar activity. At the December solstice, the RSF occurrence was 73.3% during medium solar activity and 80.8% during low solar activity. Whereas, FSF occurrence was 23.3% during medium solar activity and 63.2% during low solar activity.

RSF occurrence rate was higher during quiet geomagnetic activity (Ap $<$ 12) than during disturbed geomagnetic

Table 1
Seasonal occurrence of RSF from November 2014 to December 2019. This is the percentage of days with at least one RSF event daily in a season.

Season	2014 (%)	2015 (%)	2016 (%)	2017 (%)	2018 (%)	2019 (%)
December solstice	77.6	60.3	75.0	91.2	73.9	85.7
March equinox			28.9	38.0	82.0	
June solstice		11.5	34.4	76.7	85.7	53.2
September equinox		60.9	18.5	48.0	60.9	78.2

Table 2
Seasonal occurrence of FSF from November 2014 to December 2019.

Season	2014 (%)	2015 (%)	2016 (%)	2017 (%)	2018 (%)	2019 (%)
December solstice	30.6	13.8	81.7	74.5	52.2	45.2
March equinox			26.3	50.0	72.1	
June solstice		7.7	25.0	61.7	58.6	33.8
September equinox		21.9	24.1	42.0	43.5	45.5

activity (Ap $\geq$ 12) in all seasons except in June solstice (Fig. 14). FSF was most seen under quiet geomagnetic conditions for September equinox and December solstice, and during disturbed conditions for June solstice and March equinox. In March equinox, under disturbed conditions, the FSF occurrence rate was higher than the RSF occurrence rate. The opposite was observed in the other seasons.

3.3. Plasma bubbles occurrence rate

Fig. 15 depicts an example of TEC depletions along satellites Pseudorandom Numbers (PRNs) 19 and 16 arcs for 20/11/2014. These plasma bubble signatures appeared at 22–1 LT, except in June solstice 2017 (0–3 LT) and December solstice 2018 (2–6 LT). Table 3 shows the sea-

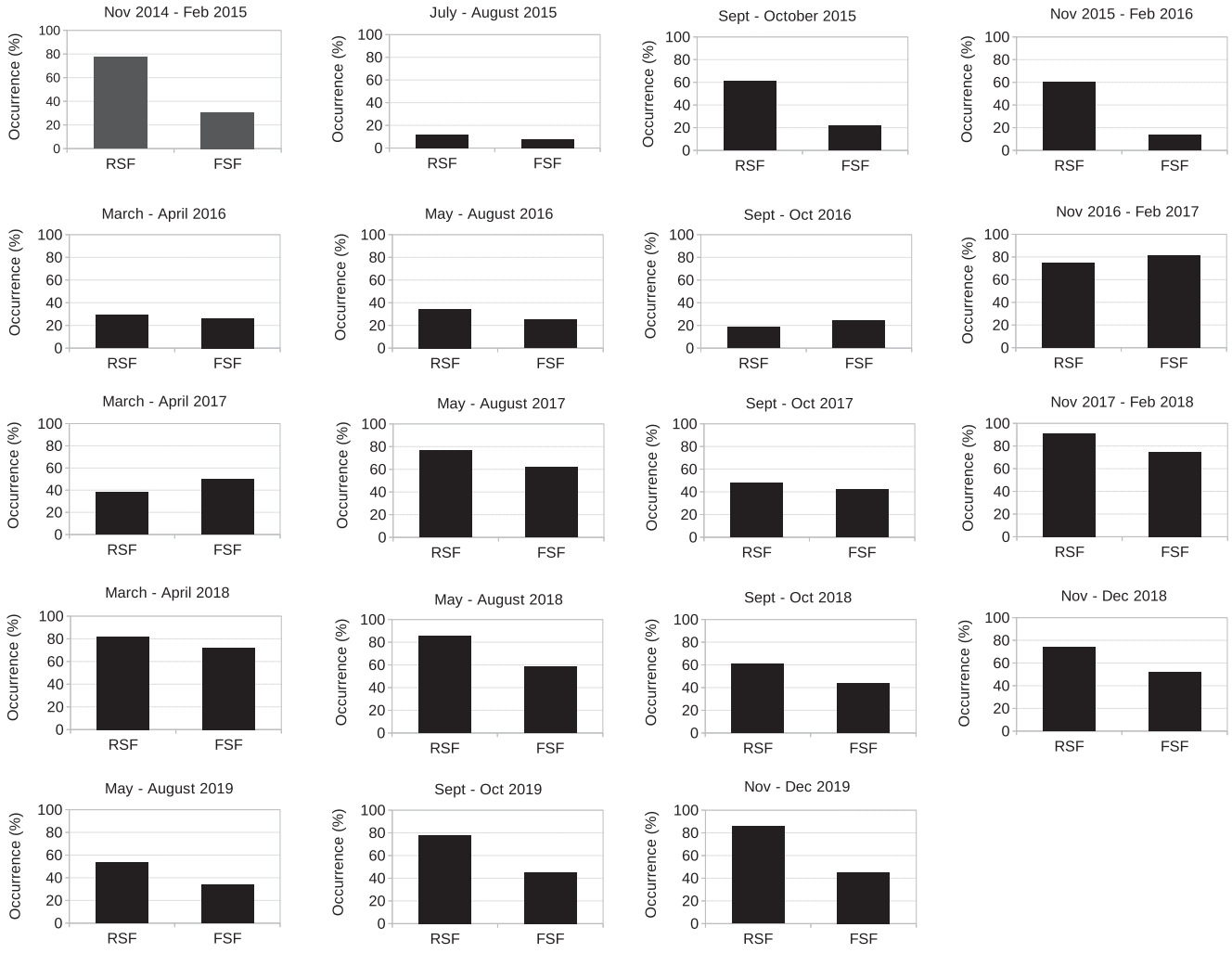

Fig. 10. Seasonal occurrence rate of different types of spread-F (RSF and FSF) in Tucumán from November 2014 to December 2019.

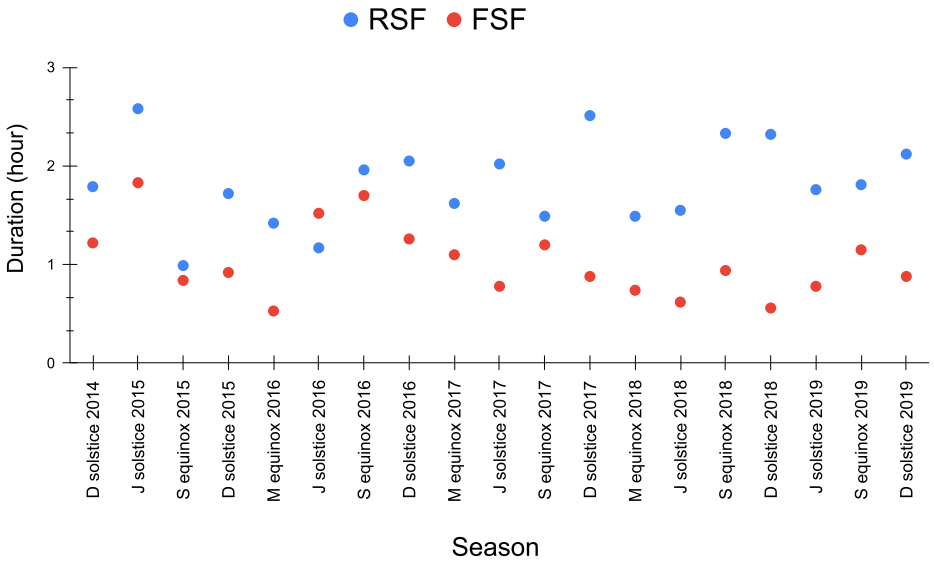

Fig. 11. Seasonal variation of the mean RSF (blue) and FSF (red) duration in Tucumán from November 2014 to December 2019 (M: March, J: June, S: September, D: December). (For interpretation of the references to colour in this figure legend, the reader is referred to the web version of this article.)

sonal occurrence of TEC depletions for the period considered. We observed a high occurrence of plasma bubbles in the December solstice (summer in the Southern Hemisphere) and a low occurrence in the June solstice (winter in the Southern Hemisphere). We did not see any plasma bubbles in June solstice 2015 and 2018 (Fig. 16a).

There were no days with high solar activity in March and September equinox. During the June solstice, the days with high solar activity levels did not present TEC depletion. In all seasons, plasma bubble occurrence increased with the F10.7 index (Fig. 16b). The period with the highest plasma bubble occurrence percentage was December solstice during high solar activity (80%). Whereas the lowest occurrence was in the June solstice during low solar activity (0.4%).

Under low solar activity levels (Fig. 16c), plasma bubble occurrence enhanced on disturbed days in all seasons except in June solstice when no plasma bubble was observed. Under medium solar activity (Fig. 16d), plasma bubble occurrence rate increased with geomagnetic activity

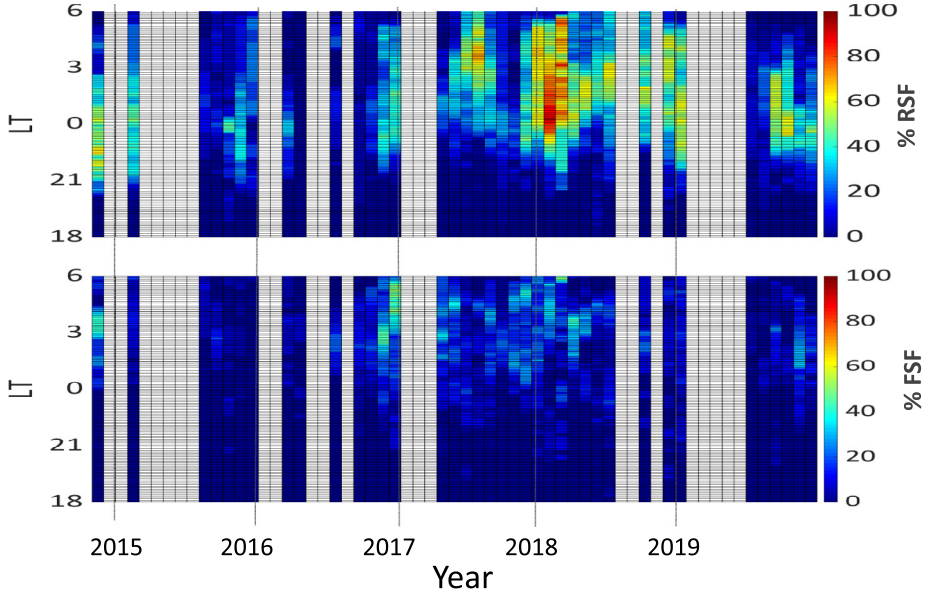

Fig. 12. Monthly mean of RSF (top) and FSF (bottom) occurrence percentages in Tucumán from November 2014 to December 2019. Grey regions indicate data gaps.

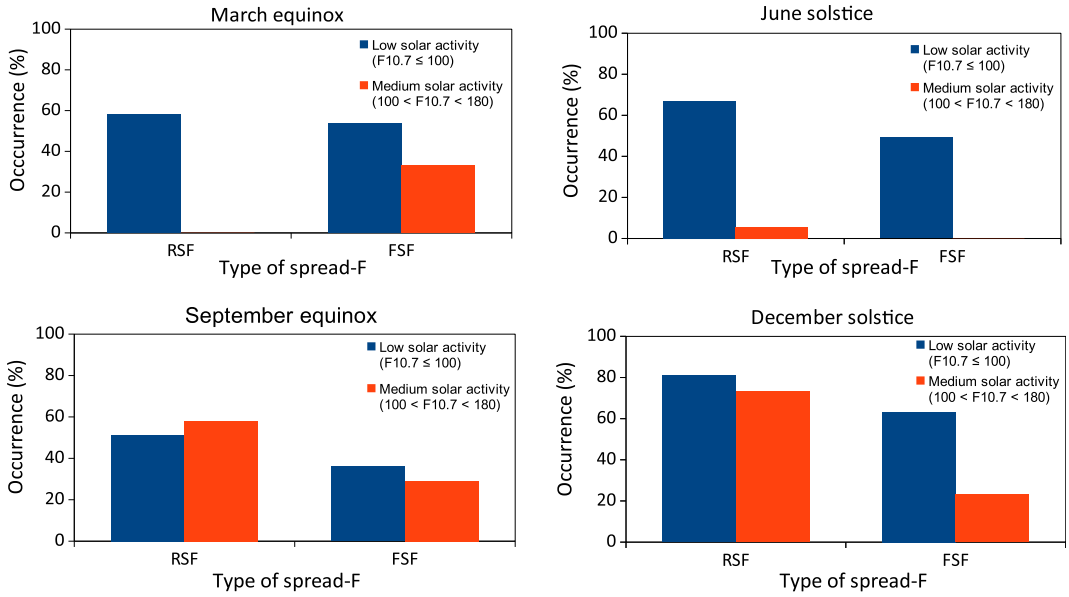

Fig. 13. Occurrence rates of two types of spread-F under low (blue) and medium (orange) solar activity levels in Tucumán during November 2014 – December 2019. (For interpretation of the references to colour in this figure legend, the reader is referred to the web version of this article.)

in all seasons but in December solstice. For the latter, plasma bubble occurrence during quiet days (38.7%) was higher than during disturbed days (29.4%).

4. Discussion

4.1. Range spread-F and frequency spread-F occurrence characteristics

According to our results, RSF was the most common type of spread-F over Tucumán during the descending phase of Solar Cycle 24. It frequently developed around local midnight (except during June solstice when its occurrence peaked later). Whereas FSF events usually occurred after midnight. All spread-F events lasted less than three hours and in years of low solar activity, the RSF duration peaked in local summer. We observed a maximum spread-F (RSF and FSF) occurrence rate in December solstice (local summer) and a minimum in equinox. These results are inconsistent with the solar terminator-magnetic field alignment hypothesis (Abdu et al., 1981a; Tsunoda 1985). This hypothesis states that the occurrence of irregularities maximizes when sunset at the conjugate E-regions is nearly simultaneous, that is when the sunset terminator is aligned

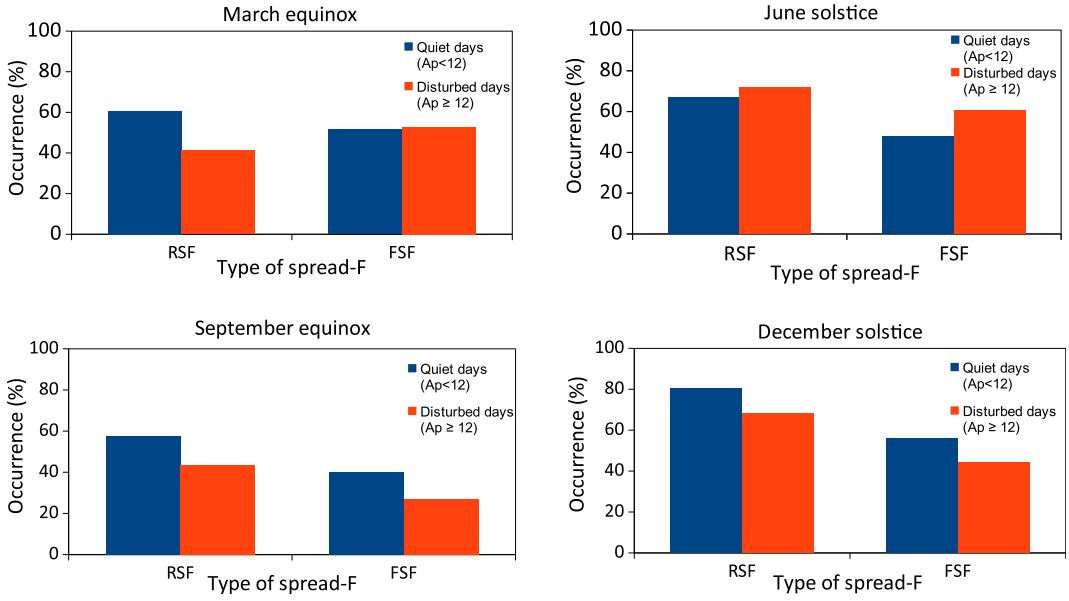

Fig. 14. Occurrence rates of two types of spread-F under quiet (blue) and disturbed (orange) geomagnetic conditions in Tucumán during November 2014 – December 2019. (For interpretation of the references to colour in this figure legend, the reader is referred to the web version of this article.)

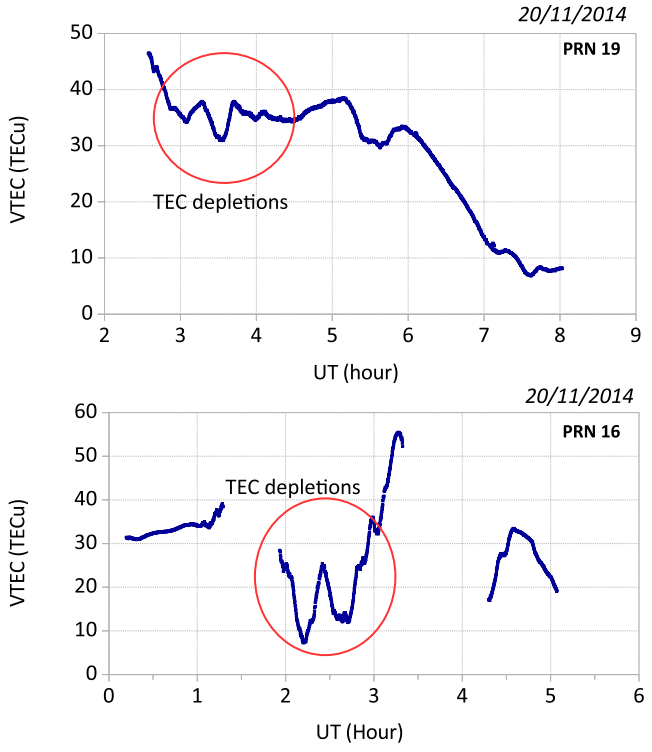

Fig. 15. Plasma bubbles signatures (TEC depletion) in Tucumán during 20/11/14 for PRN 19 (top) and PRN 16 (bottom).

with the magnetic meridian. In Tucumán, the magnetic declination angle is ~ 7°W and close alignment occurs in the equinoxes however we observed a maximum in local summer. Tsunoda et al. (2015) discussed similar observations for Africa, and the central Pacific region.

The spread-F seasonal distribution found in our work agree with some previous studies carried out in the American sector. Abdu et al. (1998) showed that, at Tucumán, spread-F occurs mainly around November–December and also extends to equinoxes with large variability from year to year. From Figs. 4 to 8, it is possible to observe that this annual variability also seems to be present in our results. Alfonsi et al. (2013) reported a maximum spread-F occurrence in local summer in Tucumán from October 2010 to September 2011. Using continuous Doppler sounding, Chum et al. (2016) reported that most of the spread F events over Tucumán were observed during local summer. Chen et al. (2006) described the equatorial F region irregularities in two Peruvian stations from April 1999 to March 2000. They observed that the night-time occurrences of spread-F were higher at the December solstice than at the Equinox. Abdu et al. (2000) studied the spread-F characteristics at two Brazilian stations; Fortaleza, an equatorial station, and Cachoeira Paulista, a low latitude station. They found that, in agreement with our results, the spread-F occurrence was maximum around the December solstice. Also in Brazil, Afolayan et al. (2019) reported higher RSF occurrence in the December solstice than in other seasons. In addition, Chandra et al. (2003) found a maximum spread-F occurrence in local summer in Huancayo (an equatorial station in Peru) and Cachoeria Paulista (at the southern crest of the EIA in Brazil) during 1983–1995. Similar results were also described by Dabas et al. (2007) at a low latitude station in the Indian region. On the contrary, in the Thailand sector, Rungraengwajiake et al. (2013) showed that the RSF occurrence is higher in the equinoctial months than in other months. Furthermore, our results evince a solstice asymmetry, that is, higher occurrence rates in the December solstice than in the June solstice. Nishioka et al. (2008) proposed that the seasonal variation of the flux tube integrated conductivities in the F-regions could partially explain this behaviour.

The response of RSF and FSF to geomagnetic activity varied with the season: we generally observed a suppression during equinox and summer but an enhancement during winter. Our results are partially consistent with those of Whalen (2002), who used an array of ionospheric sounders in the western South American sector during solar maximum and showed that spread-F decrease with increasing Kp during equinox and summer, but they found no correlation in winter. Our observation of an increase of spread-F in winter agrees with Rastogi et al. (1981). They showed that at Huancayo, Peru, spread-F was more frequent on disturbed than on quiet days during the June solstice (local winter). Lan et al. (2019) analysed ionograms recorded at the northern equatorial ionization anomaly in China. They reported a positive correlation for all types of spread-F in winter, and for RSF in all seasons, whereas the found an inverse correlation for FSF in summer. We observed a similar behaviour for FSF. In contrast, RSF was negatively correlated with geomagnetic activity in all seasons except in June solstice.

Spread-F suppression/generation may be a consequence of the effect of the magnetic activity on the E × B velocity, hence in the vertical growth of the irregularities. Electric field perturbations associated with the solar wind-magnetosphere dynamo or with the ionospheric disturbance dynamo (Blanc and Richmond, 1980; Senior and Blanc, 1984) can significantly modify the low-latitude elec-

Table 3
Seasonal occurrence of TEC depletions from November 2014 to December 2019.

Season	2014 (%)	2015 (%)	2016 (%)	2017 (%)	2018 (%)	2019 (%)
December solstice	43.3	23.2	15.1	6.0	3.4	
March equinox		8.2	1.6	2.3	1.8	4.2
June solstice		0	0.9	2.3	0	
September equinox		11.5	11.9	48.0	1.6	

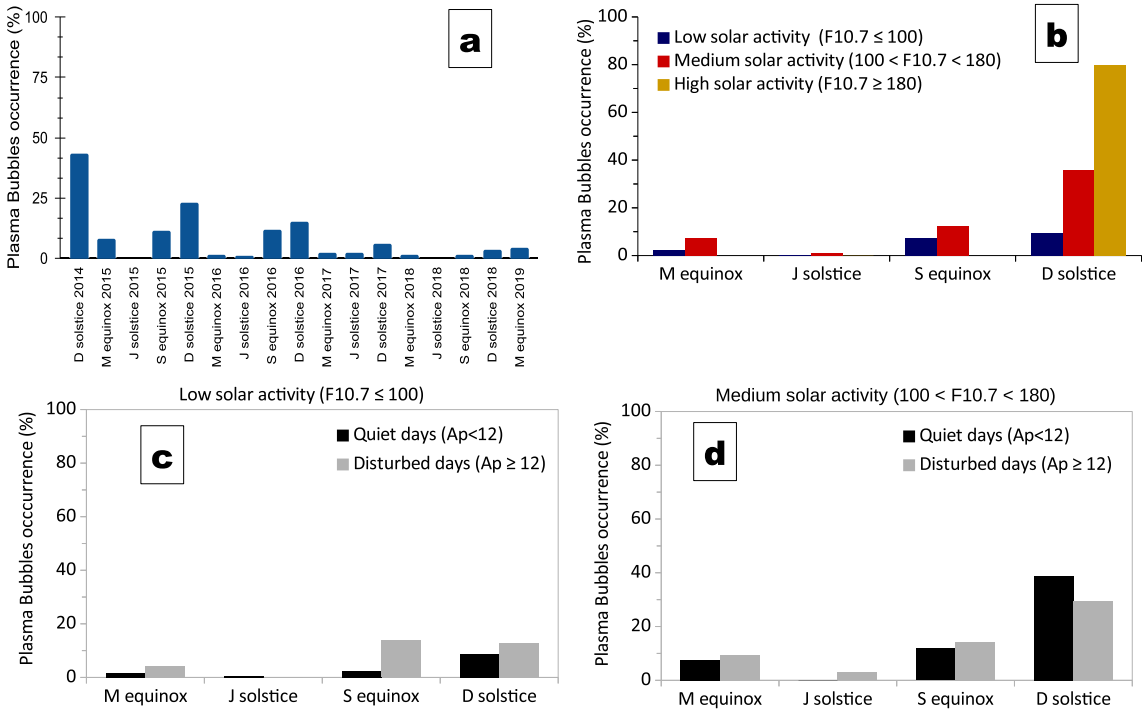

Fig. 16. (a) Seasonal variation of the occurrence of Plasma Bubbles over Tucumán for the period November 2014 – March 2019 (M: March, J: June, S: September, D: December). (b) Plasma bubbles occurrence rate under low (dark blue), medium (orange) and high (yellow) solar activity levels. (c) Plasma bubbles occurrence rate under quiet (black) and disturbed (grey) geomagnetic conditions under low solar activity. (d) Same as (c) but under medium solar activity. (For interpretation of the references to colour in this figure legend, the reader is referred to the web version of this article.)

tric fields during disturbed geomagnetic conditions. Depending upon their local time-dependent polarity, these disturbance electric fields could increase the plasma vertical drift—because of a stronger eastward electric field—and uplift the F layer to heights with reduced collision frequency and thus enhance the instability growth. Depending on the time (UT) of the main and recovery phases of the storm, RSF can be enhanced or suppressed. A westward disturbance electric field can cause plasma downdraft and a drop in the F layer height that may induce a suppression or disruption in the irregularity development. Therefore, the response of spread-F to geomagnetic activity depends on the location of the station, the season, and the phase of the storm.

We observed that the spread-F occurrence decreased with solar flux in all seasons, except for RSF on the September equinox. It is important to note that, for the period analysed, the range of values of F10.7 is small, and we cannot draw a reliable conclusion on the dependence of spread-F and plasma bubbles with solar activity. Furthermore, due to the lack of ionosonde data, it was not possible to examine the entire solar cycle. Some researchers reported a negative correlation with the F10.7 index. Chandra and Rastogi (1970) found that spread-F varies inversely with sunspot number in the South American sector. Chandra et al. (2003) found that at Huancayo (Peru) spread-F was more frequent during low sunspot years. The opposite was observed in the Indian sector. (Wang et al., 2018) used data from four ionosondes at low- and mid-latitudes in China and found that the FSF occurrence percentages were higher during the low solar activity years. On the other hand, some studies disagree with these observations. Abdu et al. (2000) examined the solar activity control of spread-F in Brazil. They observed a positive dependence during the post-sunset hours over a low latitude station. They attributed this to a higher mean plasma bubble rise velocity at the equator. Klinngam et al. (2015) studied the spread-F occurrence at low latitudes in Southeast Asia, they showed that the percentage of RSF occurrence increased with the level of solar activity, while the FSF occurrence decreased. Thammavongsy et al. (2020) studied the spread-F occurrence percentage during the peak of solar cycle 24 at Chumphon station, Thailand. They concluded that the tendency of the RSF occurrence rate was proportional to the F10.7 solar flux. The disparity in the results reported in the literature highlights the complexity of this ionospheric phenomenon. The difference in the observations may be related to the effects of the thermospheric zonal wind and the atmospheric waves that alter the primary parameters important for spread-F formation.

4.2. Plasma bubbles occurrence characteristics

The seasonal variation pattern in the plasma bubble (TEC depletion) occurrence rate observed in the present work–high occurrence during local summer and low occurrence during winter–agree with previous studies carried out in South America. Sahai et al. (1994) used OI 630.0 nm

imaging observations over the southern crest of the EIA in Brazil and found that airglow depletions were higher from October through March and lower from April through September. Barros et al. (2018) used TEC maps over South America and found that plasma bubbles occurred mainly from September to March. They defined plasma bubbles as TEC depletions with an amplitude exceeding 10 TECU.

During the descending phase of solar cycle 24 plasma bubble occurrence rate was positively correlated with solar activity. This behaviour agrees with previous studies over the Brazilian and Indian regions (Abdu et al., 1985; Shetti et al., 2019). Sahai et al. (2000) used OI 630 nm all-sky imaging observations from Cachoeria Paulista in Brazil, they showed that plasma bubble occurrence was lower during low solar activity as compared with high solar activity from October to March. It is important to note that we expect the background TEC to decrease with solar activity, so the threshold value (5 TECU) used in this work to detect TEC depletion associated with plasma bubbles becomes more difficult to achieve. This could be a reason for the low number of TEC depletions observed during years of low solar activity.

The plasma bubble occurrence rate was generally higher on disturbed days than on quiet days. However, under medium solar activity, we observed that during the high plasma bubbles occurrence season (December solstice, summer in the Southern Hemisphere), days with disturbed geomagnetic activity registered fewer TEC depletions. Whereas, in the low plasma bubbles occurrence season (June solstice, winter in the Southern Hemisphere), the plasma bubble occurrence rate was higher during disturbed conditions. These results agree with Becker-Guedes et al. (2004) who proposed that, in Brazil, geomagnetic activity inhibits plasma bubbles generation during high plasma bubbles occurrence season, and helps in the initiation process during low occurrence season. Timoçin et al. (2020) investigated the behaviour of plasma bubble irregularities under different geomagnetic conditions during March 2015 and September 2017 at three low latitudes stations in the Indian sector. They observed that the plasma bubble occurrence rate increased with geomagnetic activity, in concordance with our results.

4.3. Comparison between the occurrence characteristics of plasma bubbles and RSF

During June solstice, RSF occurrence steadily increased from 2015 to 2018 (when the occurrence rate reached over 80%) as the mean F10.7 and Ap index decreased. However, plasma bubbles were very few in June solstice (<2.3%) and were absent in 2015 and 2018 during this season, as seen from TEC depletions. At low latitudes, RSF in ionograms usually indicates plasma bubbles originated around sunset at the magnetic equator that expanded to higher latitudes along the magnetic field lines (Abdu et al., 1998). To be detected in Tucumán, the strength of the equatorial evening E × B drift (due to the pre-reversal enhancement, PRE) should be strong enough for the bubble to reach a high apex altitude over the magnetic equator. Previous studies attributed the low plasma bubble occurrence during June solstice to a weak equatorial electric field pre-reversal enhancement over South America (Batista et al., 1996; Fejer et al., 1999). Sahai et al. (2000) analysed the OI 630 nm all-sky imaging data from Cachoeira Paulista, Brazil (a location at the southern crest of the EIA) and found that plasma bubbles attaining high apex heights (≥1500 km) at the magnetic equator were more abundant during high solar activity (66%) compared with low solar activity (34%). Lee et al. (2009) investigated the occurrence of F region irregularities at the EIA crest during solar maximum and concluded that the possibility for irregularities to extend from the dip equator to the EIA crest was about 50%. So it is reasonable to think that the RSF observed in the June solstice during low solar activity may be associated with other phenomena rather than plasma bubbles.

During low solar activity and quiet geomagnetic conditions, and when the PRE is small (as in June solstice), the gravity waves may play a significant role in the spread-F seeding process. Candido et al. (2011) reported a low occurrence of spread-F during June solstice at high solar activity years and a progressive increase during moderate and low solar flux conditions at Cachoeira Paulista. They observed a frequent occurrence of spread-F in June solstice during solar minimum activity and mainly under quiet geomagnetic conditions. They suggested that these events could be caused by ionospheric disturbances unrelated to equatorial processes such as travelling ionospheric disturbances (TIDs) from mid-latitudes. Cabrera et al. (2010) evaluated the RSF day-to-day variability in September 2007 (low solar activity) at Tucumán. They argued that locally generated plasma instabilities related to gravity waves triggered by the solar terminator could cause RSF rather than plasma bubbles coming from the magnetic equator. Pezzopane et al. (2013) analysed four equinoctial months in a year of low solar activity and found that satellite traces caused by gravity waves propagation are a precursor to the RSF appearance at Tucumán. Afolayan et al. (2019) attributed the large RSF occurrence percentage during low solar activity in the West African region to the presence of gravity waves. Furthermore, the amplitude of the gravity wave seed perturbation decides whether spread-F would form. The neutral density decreases as the solar flux decreases, so lower seed magnitude for spread-F occurrence is needed as solar activity decreases (Manju et al., 2016). A possibility is that the RSF signatures seen in the ionograms in Tucumán during winter in low solar activity can be related to night-time medium-scale TIDs (MSTIDs).

Many studies have proposed that the MSTIDs may contribute to the generation of spread-F at low latitudes. Polarization electric fields associated with gravity wave-driven MSTIDs can trigger the Rayleigh-Taylor instability and caused spread-F (Miller et al., 2009; Oliver et al., 1997). Alfonsi et al. (2013) studied ionosonde data from

Tucumán during October 2010-September 2011 (a period of low-medium solar activity). They concluded that exist a connection between RSF occurrence and medium-scale TIDs due to gravity wave propagation. Lan et al. (2019) suggested that night-time MSTIDs might play a significant role in the occurrence of RSF and FSF over Puer, China, at the northern crest of the EIA. Moreover, Pimenta et al. (2008) showed that, in the Brazilian region, night-time spread-F can be caused by night-time mid-latitudes MSTIDs that propagate toward low latitudes. Recently, Deng et al. (2021) analysed the mechanism of MSTIDs inducing spread-F at low latitudes in South America. They found that post-midnight MSTIDs tend to trigger spread-F, also they suggested MSTIDs triggered by Perkins instability would show a further tendency to generate spread-F. Tucumán is at the boundary between low latitude and mid-latitude, it is reasonable to suggest that some of the RSF events may be associated with mid-latitude night-time MSTIDs.

The vertical plasma drift and the ensuing F layer uplift are important conditions for the development of ionospheric irregularities. Thus, ionospheric parameters e.g. the virtual height of the F layer bottom side (h'F), the F layer peak height (hmF2) or the critical frequency of the F2 layer (foF2) are needed to further examine the precursor conditions that may lead to spread-F generation. With this in mind, we are developing software that allows us to get automatically these parameters from the VIPIR ionograms. Another basic condition to start the instability growth is a source of density perturbations, such as gravity waves. To further study the role of these seed perturbations on the day-to-day variability of spread-F, case studies combining ground-based and space-borne observations are required.

5. Conclusion

We analysed the RSF, FSF and TEC depletion occurrence at Tucumán, a station near the southern crest of the EIA during the descending phase of Solar Cycle 24. The main outcomes of this work are:

1. RSF was the most frequent type of spread-F in Tucumán.
2. Spread-F and plasma bubble occurrence rates were maximum in local summer, but in 2018 the highest RSF occurrence was in winter.
3. Plasma bubble and spread-F occurrence rates were minimum in winter and equinox, respectively.
4. RSF and FSF occurrence generally decreased under disturbed geomagnetic conditions in equinox and December solstice. Whereas it increased in June solstice.
5. Under low solar activity, there was a positive correlation between plasma bubble occurrence and geomagnetic activity. Whereas, under medium solar activity, there was a negative correlation in December solstice and a positive one in all the other seasons.
6. RSF signatures observed in winter under low solar activity were not related to plasma bubbles originated at the magnetic equator. A possibility is that these irregularities were associated with night-time MSTIDs. This needs to be further analysed.

Declaration of Competing Interest

The authors declare that they have no known competing financial interests or personal relationships that could have appeared to influence the work reported in this paper.

Acknowledgment

The Low Latitude Ionospheric Sensor Network (LISN) is funded by NSF Grant AGS-1933056 and is a project led by the University of Texas at Dallas in collaboration with the Geophysical Institute of Peru and other institutions that provide information in benefit of the space weather scientific community. We thank all organizations and persons that are supporting and operating VIPIR ionosondes and GPS receivers under the LISN project. The author also thanks to the following groups for making the data available: Royal Observatory of Belgium, National Research Council Canada, and the GFZ German Research Centre for Geosciences. Thanks to Dr Victor Ríos and Dr César Valladares, who are in charge of the VIPIR ionosonde installed in Tucumán.

Reference

Abdu, M.A., Bittencourt, J.A., Batista, I.S., 1981a. Magnetic declination control of the equatorial F region dynamo electric field development and spread F. J. Geophys. Res. 86 (A13), 11443. https://doi.org/10.1029/JA086iA13p11443.

Abdu, M.A., Batista, I.S., Bittencourt, J.A., 1981b. Some characteristics of spread F at the magnetic equatorial station Fortaleza. J. Geophys. Res. 86 (A8), 6836. https://doi.org/10.1029/JA086iA08p06836.

Abdu, M., Sobral, J.H., Nelson, O., Batista, I., 1985. Solar cycle related range type spread-F occurrence characteristics over equatorial and low latitude stations in Brazil. J. Atmos. Terr. Phys. 47 (8–10), 901–905. https://doi.org/10.1016/0021-9169(85)90065-0.

Abdu, M.A., Sobral, J.H.A., Batista, I.S., Rios, V.H., Medina, C., 1998. Equatorial spread-F occurrence statistics in the American longitudes: Diurnal, seasonal and solar cycle variations. Adv. Space Res. 22 (6), 851–854. https://doi.org/10.1016/S0273-1177(98)00111-2.

Abdu, M.A., Sobral, J.H.A., Batista, I.S., 2000. Equatorial spread F statistics in the American longitudes: Some problems relevant to ESF description in the IRI scheme. Adv. Space Res. 25 (1), 113–124. https://doi.org/10.1016/S0273-1177(99)00907-2.

Abdu, M.A., Souza, J.R., Batista, I.S., Sobral, J.H.A., 2003. Equatorial spread F statistics and empirical representation for IRI: a regional model for the Brazilian longitude sector. Adv. Space Res. 31 (3), 703–716. https://doi.org/10.1016/S0273-1177(03)00031-0.

Afolayan, A.O., Jit Singh, M., Abdullah, M., Buhari, S.M., Yokoyama, T., Supnithi, P., 2019. Observation of seasonal asymmetry in the range spread F occurrence at different longitudes during low and moderate solar activity. Ann. Geophys. 37 (4), 733–745. https://doi.org/10.5194/angeo-37-733-2019.

Alfonsi, L., Spogli, L., Pezzopane, M., Romano, V., Zuccheretti, E., De Franceschi, G., Ezquer, R.G., 2013. Comparative analysis of spread-F

signature and GPS scintillation occurrences at Tucumán, Argentina. J. Geophys. Res. Space Phys. 118 (7), 4483–4502. https://doi.org/10.1002/jgra.50378.
Anderson, D.N., Haerendel, G., 1979. The motion of depleted plasma regions in the equatorial ionosphere. J. Geophys. Res. Space Phys. 84 (A8), 4251–4256. https://doi.org/10.1029/JA084iA08p04251.
Aquino, M., Sreeja, V., 2013. Correlation of scintillation occurrence with interplanetary magnetic field reversals and impact on global navigation satellite system receiver tracking performance. Space Weather 11 (5), 219–224. https://doi.org/10.1002/swe.20047.
Balan, N., Liu, L., Le, H., 2018. A brief review of equatorial ionization anomaly and ionospheric irregularities. Earth Planet. Phys. 2 (4), 1–19 https://doi.org/10.26464/epp2018025.
Balsley, B.B., Haerendel, G., Greenwald, R.A., 1972. Equatorial spread F: recent observations and a new interpretation. J. Geophys. Res. 77 (28), 5625–5628. https://doi.org/10.1029/JA077i028p05625.
Barros, D., Takahashi, H., Wrasse, C.M., Figueiredo, C.A.O.B., 2018. Characteristics of equatorial plasma bubbles observed by TEC map based on ground-based GNSS receivers over South America. Ann. Geophys. 36 (1), 91–100. https://doi.org/10.5194/angeo-36-91-2018.
Batista, I.S., de Medeiros, R.T., Abdu, M.A., de Souza, J.R., Bailey, G.J., de Paula, E.R., 1996. Equatorial ionospheric vertical plasma drift model over the Brazilian region. J. Geophys. Res. Space Phys. 101 (A5), 10887–10892. https://doi.org/10.1029/95JA03833.
Becker-Guedes, F., Sahai, Y., Fagundes, P.R., Lima, W.L.C., Pillat, V.G., Abalde, J.R., Bittencourt, J.A., 2004. Geomagnetic storm and equatorial spread-F. Ann. Geophys. 22 (9), 3231–3239. https://doi.org/10.5194/angeo-22-3231-2004.
Blanc, M., Richmond, A.D., 1980. The ionospheric disturbance dynamo. Journal of Geophysical Research 85 (A4), 1669–1686. https://doi.org/10.1029/JA085iA04p01669, In this issue.
Booker, G., Wells, H.W., 1938. Scattering of radio waves by the F-region of the ionosphere. J. Geophys. Res. 43, 249–256 https://agupubs.onlinelibrary.wiley.com/doi/abs/10.1029/TE043i003p00249.
Bowman, G.G., Mortimer, I.K., 2003. Influence of geomagnetic activity on the occurrence of midlatitude ionogram-recorded spread-F. Indian J. Radio Space Phys. 32 (1), 16–20.
Bullett, T., 2008. Station Report : A New Ionosonde at Boulder. Retrieved from https://www.sws.bom.gov.au/IPSHosted/INAG/web-69/2008/boulder_vipir.pdf.
Cabrera, M.A., Pezzopane, M., Zuccheretti, E., Ezquer, R.G., 2010. Satellite traces, range spread-F occurrence, and gravity wave propagation at the southern anomaly crest. Ann. Geophys. 28 (5), 1133–1140. https://doi.org/10.5194/angeo-28-1133-2010.
Calvert, W., 1963. Instability of the equatorial F layer after sunset. J. Geophys. Res. 68 (9), 2591–2593. https://doi.org/10.1029/JZ068i009p02591.
Candido, C.M.N., Batista, I.S., Becker-Guedes, F., Abdu, M.A., Sobral, J.H.A., Takahashi, H., 2011. Spread F occurrence over a southern anomaly crest location in Brazil during June solstice of solar minimum activity. J. Geophys. Res. Space Phys. 116 (6), 2008–2009. https://doi.org/10.1029/2010JA016374.
Çepni, M.S., Potts, L.V., Miima, J.B., 2013. High-resolution station-based diurnal ionospheric total electron content (TEC) from dual-frequency GPS observations. Space Weather 11 (9), 520–528. https://doi.org/10.1002/swe.20093.
Chandra, H., Rastogi, R.G., 1970. Solar cycle and seasonal variation of spread-F near the magnetic equator. J. Atmos. Terr. Phys. 32 (3), 439–443. https://doi.org/10.1016/0021-9169(70)90019-X.
Chandra, H., Sharma, S., Abdu, M.A., Batista, I.S., 2003. Spread-F at anomaly crest regions in the Indian and American longitudes. Adv. Space Res. 31 (3), 717–727. https://doi.org/10.1016/S0273-1177(03)00034-6.
Chen, W.S., Lee, C.C., Liu, J.Y., Chu, F.D., Reinisch, B.W., 2006. Digisonde spread F and GPS phase fluctuations in the equatorial ionosphere during solar maximum. J. Geophys. Res. Space Phys. 111 (12), 1–9. https://doi.org/10.1029/2006JA011688.
Chum, J., Liu, J.Y., Chen, S.P., Cabrera, M.A., Laštovička, J., Baše, J., Ezquer, R., 2016. Spread F occurrence and drift under the crest of the equatorial ionization anomaly from continuous Doppler sounding and FORMOSAT-3/COSMIC scintillation data. Earth Planets Space 68 (1), 1–18. https://doi.org/10.1186/s40623-016-0433-1.
Cueva, R.Y.C., De Paula, E.R., Kherani, A.E., 2013. Statistical analysis of radar observed F region irregularities from three longitudinal sectors. Ann. Geophys. 31 (12), 2137–2146. https://doi.org/10.5194/angeo-31-2137-2013.
Dabas, R.S., Das, R.M., Sharma, K., Garg, S.C., Devasia, C.V., Subbarao, K.S.V., Rama Rao, P.V.S., 2007. Equatorial and low latitude spread-F irregularity characteristics over the Indian region and their prediction possibilities. J. Atmos. Sol. Terr. Phys. 69 (6), 685–696. https://doi.org/10.1016/j.jastp.2007.01.002.
DasGupta, A., Basu, S., Aarons, J., Klobuchar, J.A., Basu, S., Bushby, A., 1983. VHF amplitude scintillations and associated electron content depletions as observed at Arequipa, Peru 15–19, 21–26. J. Atmos. Terrestrial Phys. 45 (1) http://www.sciencedirect.com/science/article/pii/S0021916983800038.
Dashora, N., Pandey, R., 2005. Observations in equatorial anomaly region of total electron content enhancements and depletions. Ann. Geophys. 23 (7), 2449–2456. https://doi.org/10.5194/angeo-23-2449-2005.
Deng, Z., Wang, R., Liu, Y., Xu, T., Wang, Z., Chen, G., Zhou, C., 2021. Investigation of low latitude spread-F triggered by nighttime medium-scale traveling ionospheric disturbance. Remote Sens. 13 (5), 945. https://doi.org/10.3390/rs13050945.
Dungey, J.W., 1956. Convective diffusion in the equatorial F region. J. Atmos. Terr. Phys. 9 (5–6), 304–310. https://doi.org/10.1016/0021-9169(56)90148-9.
Farley, D.T., Balsley, B.B., Woodman, R.F., McClure, J.P., 1970. Equatorial spread F: implications of VHF radar observations. J. Geophys. Res. 75 (34), 7199–7216. https://doi.org/10.1029/JA075i034p07199.
Fejer, B.G., Scherliess, L., de Paula, E.R., 1999. Effects of the vertical plasma drift velocity on the generation and evolution of equatorial spread F. J. Geophys. Res. Space Phys. 104 (A9), 19859–19869. https://doi.org/10.1029/1999JA900271.
Klinngam, S., Supnithi, P., Rungraengwajiake, S., Tsugawa, T., Ishii, M., Maruyama, T., 2015. The occurrence of equatorial spread-F at conjugate stations in Southeast Asia. Adv. Space Res. 55 (8), 2139–2147. https://doi.org/10.1016/j.asr.2014.10.003.
Kotulak, K., Zakharenkova, I., Krankowski, A., Cherniak, I., Wang, N., Fron, A., 2020. Climatology characteristics of ionospheric irregularities described with GNSS ROTI. Remote Sens. 12 (16), 2634. https://doi.org/10.3390/rs12162634.
Lan, T., Jiang, C., Yang, G., Zhang, Y., Liu, J., Zhao, Z., 2019. Statistical analysis of low-latitude spread F observed over Puer, China, during 2015–2016. Earth Planets Space 71 (1), 138. https://doi.org/10.1186/s40623-019-1114-7.
Lee, C.C., Chu, F.D., Chen, W.S., Liu, J.Y., Su, S.-Y., Liou, Y.A., Yu, S. B., 2009. Spread F, GPS phase fluctuations, and plasma bubbles near the crest of equatorial ionization anomaly during solar maximum. J. Geophys. Res.: Space Phys. 114 (A8), n/a-n/a. https://doi.org/10.1029/2009JA014195.
Li, Q., Zhu, Y., Fang, K., Fang, J., 2020. Statistical study of the seasonal variations in TEC depletion and the ROTI during 2013–2019 over Hong Kong. Sensors 20 (21), 6200. https://doi.org/10.3390/s20216200.
Magdaleno, S., Herraiz, M., de la Morena, B.A., 2012. Characterization of equatorial plasma depletions detected from derived GPS data in South America. J. Atmos. Sol. Terr. Phys. 74, 136–144. https://doi.org/10.1016/j.jastp.2011.10.014.
Manju, G., Madhav Haridas, M.K., Aswathy, R.P., 2016. Role of gravity wave seed perturbations in ESF day-to-day variability: a quantitative approach. Adv. Space Res. 57 (4), 1021–1028. https://doi.org/10.1016/j.asr.2015.12.019.

Mendillo, M., Tyler, A., 1983. Geometry of depleted plasma regions in the equatorial ionosphere. J. Geophys. Res. 88 (A7), 5778. https://doi.org/10.1029/JA088iA07p05778.

Miller, E.S., Makela, J.J., Kelley, M.C., 2009. Seeding of equatorial plasma depletions by polarization electric fields from middle latitudes: experimental evidence. Geophys. Res. Lett. 36 (18), 1–5. https://doi.org/10.1029/2009GL039695.

Muella, M.T.A.H., Kherani, E.A., De Paula, E.R., Cerruti, A.P., Kintner, P.M., Kantor, I.J., Abdu, M.A., 2010. Scintillation-producing Fresnel-scale irregularities associated with the regions of steepest TEC gradients adjacent to the equatorial ionization anomaly. J. Geophys. Res. Space Phys. 115 (3), 1–19. https://doi.org/10.1029/2009JA014788.

Nishioka, M., Saito, A., Tsugawa, T., 2008. Occurrence characteristics of plasma bubble derived from global ground-based GPS receiver networks. J. Geophys. Res. Space Phys. 113 (5), 1–12. https://doi.org/10.1029/2007JA012605.

Oliver, W.L., Otsuka, Y., Sato, M., Takami, T., Fukao, S., 1997. A climatology of F region gravity wave propagation over the middle and upper atmosphere radar. J. Geophys. Res. Space Phys. 102 (A7), 14499–14512. https://doi.org/10.1029/97JA00491.

Pezzopane, M., Zuccheretti, E., Abadi, P., De Abreu, A.J., De Jesus, R., Fagundes, P.R., Ezquer, R.G., 2013. Low-latitude equinoctial spread-F occurrence at different longitude sectors under low solar activity. Ann. Geophys. 31 (2), 153–162. https://doi.org/10.5194/angeo-31-153-2013.

Pietrella, M., Pezzopane, M., Fagundes, P.R., de Jesus, R., Supnithi, P., Klinngam, S., Cabrera, M.A., 2017. Equinoctial spread-F occurrence at low latitudes in different longitude sectors under moderate and high solar activity. J. Atmos. Sol. Terr. Phys. 164, 149–162. https://doi.org/10.1016/j.jastp.2017.07.007.

Piggott, W.R., Rawer, K., 1978. Revision of Chapters 1–4 U.R.S.I. Handbook of Ionogram Interpretation and Reduction. Report UAG-23A (Second). World Data Cent. A for Sol. Terr. Phys, Boulder, Colorado.

Pimenta, A.A., Kelley, M.C., Sahai, Y., Bittencourt, J.A., Fagundes, P.R., 2008. Thermospheric dark band structures observed in all-sky OI 630 nm emission images over the Brazilian low-latitude sector. J. Geophysi. Res.: Space Phys. 113 (A1), n/a-n/a. https://doi.org/10.1029/2007JA012444.

Rastogi, R.G., Mullen, J.P., MacKenzie, E., 1981. Effect of geomagnetic activity on equatorial radio VHF scintillations and spread F. J. Geophys. Res. 86 (A5), 3661. https://doi.org/10.1029/JA086iA05p03661.

Reinisch, B.W., Abdu, M., Batista, I., Sales, G.S., Khmyrov, G., Bullett, T.A., Rios, V., 2004. Multistation digisonde observations of equatorial spread F in South America. Ann. Geophys. 22 (9), 3145–3153. https://doi.org/10.5194/angeo-22-3145-2004.

Röttger, J., 1973. Wave-like structures of large-scale equatorial spread-F irregularities. J. Atmos. Terr. Phys. 35 (6), 1195–1203. https://doi.org/10.1016/0021-9169(73)90016-0.

Rungraengwajiake, S., Supnithi, P., Tsugawa, T., Maruyama, T., Nagatsuma, T., 2013. The variation of equatorial spread-F occurrences observed by ionosondes at Thailand longitude sector. Adv. Space Res. 52 (10), 1809–1819. https://doi.org/10.1016/j.asr.2013.07.041.

Sahai, Y., Aarons, J., Mendillo, M., Baumgardner, J., Bittencourt, J.A., Takahashi, H., 1994. OI 630 nm imaging observations of equatorial plasma depletions at 16° S dip latitude. J. Atmos. Terr. Phys. 56 (11), 1461–1475. https://doi.org/10.1016/0021-9169(94)90113-9.

Sahai, Y., Fagundes, P.R., Bittencourt, J.A., 2000. Transequatorial F-region ionospheric plasma bubbles: solar cycle effects. J. Atmos. Sol. Terr. Phys. 62 (15), 1377–1383. https://doi.org/10.1016/S1364-6826(00)00179-6.

Seemala, G.K., Valladares, C.E., 2011. Statistics of total electron content depletions observed over the South American continent for the year 2008. Radio Sci. 46 (5), 1–14. https://doi.org/10.1029/2011RS004722.

Senior, Catherine, Blanc, Michel, 1984. On the Control of Magnetospheric Convection by the Spatial Distribution of Ionospheric Conductivities. Journal of Geophysical Research 89 (A1), 261–284. https://doi.org/10.1029/JA089iA01p00261, In this issue.

Shetti, D.J., Gurav, O.B., Seemla, G.K., 2019. Occurrence characteristics of equatorial plasma bubbles and total electron content during solar cycle peak 23rd to peak 24th over Bangalore (13.02○ N, 77.57○ E). Astrophys. Space Sci. 364 (9). https://doi.org/10.1007/s10509-019-3643-8.

Taori, A., Parihar, N., Ghodpage, R., Dashora, N., Sripathi, S., Kherani, E.A., Patil, P.T., 2015. Probing the possible trigger mechanisms of an equatorial plasma bubble event based on multistation optical data. J. Geophys. Res. Space Phys. 120 (10), 8835–8847. https://doi.org/10.1002/2015JA021541.

Thammavongsy, P., Supnithi, P., Phakphisut, W., Hozumi, K., Tsugawa, T., Bannop, K., 2020. The statistics of equatorial spread-F and effects on critical frequency at Chumphon, Thailand. In: Proceedings of the Sriwijaya International Conference on Information Technology and Its Applications (SICONIAN 2019), vol. 172. Paris, France: Atlantis Press, pp. 691–695. https://doi.org/10.2991/aisr.k.200424.105.

Timoçin, E., Inyurt, S., Temuçin, H., Ansari, K., Jamjareegulgarn, P., 2020. Investigation of equatorial plasma bubble irregularities under different geomagnetic conditions during the equinoxes and the occurrence of plasma bubble suppression. Acta Astronaut. 177 (August), 341–350. https://doi.org/10.1016/j.actaastro.2020.08.007.

Tsunoda, R.T., Towle, D.M., 1979. On the spatial relationship of 1-meter equatorial spread-F irregularities and depletions in total electron content. Geophys. Res. Lett. 6 (11), 873–876. https://doi.org/10.1029/GL006i011p00873.

Tsunoda, R.T., 1985. Control of the seasonal and longitudinal occurrence of equatorial scintillations by the longitudinal gradient in integrated E region Pedersen conductivity. J. Geophys. Res. Space Phys. 90 (A1), 447–456. https://doi.org/10.1029/JA090iA01p00447.

Tsunoda, R.T., Yamamoto, M., Tsugawa, T., Hoang, T.L., Tulasi Ram, S., Thampi, S.V., Chau, H.D., Nagatsuma, T., 2011. On seeding, large-scale wave structure, equatorial spread F, and scintillations over Vietnam. Geophys. Res. Lett. 38 (20), n/a-n/a. https://doi.org/10.1029/2011GL049173.

Tsunoda, R.T., Nguyen, T.T., Le, M.H., 2015. Effects of tidal forcing, conductivity gradient, and active seeding on the climatology of equatorial spread F over Kwajalein. J. Geophys. Res. Space Phys. 120 (1), 632–653. https://doi.org/10.1002/2014JA020762.

Valladares, C.E., Hanson, W.B., McClure, J.P., Cragin, B.L., 1983. Bottomside sinusoidal irregularities in the equatorial F region. J. Geophys. Res. 88 (A10), 8025. https://doi.org/10.1029/JA088iA10p08025.

Valladares, C.E., Villalobos, J., Sheehan, R., Hagan, M.P., 2004. Latitudinal extension of low-latitude scintillations measured with a network of GPS receivers. Ann. Geophys. 22 (9), 3155–3175. https://doi.org/10.5194/angeo-22-3155-2004.

Yizengaw, E., Groves, K.M., 2018. Longitudinal and seasonal variability of equatorial ionospheric irregularities and electrodynamics. Space Weather 16 (8), 946–968. https://doi.org/10.1029/2018SW001980.

Yokoyama, T., Fukao, S., Yamamoto, M., 2004. Relationship of the onset of equatorial F region irregularities with the sunset terminator observed with the Equatorial Atmosphere Radar. Geophys. Res. Lett. 31 (24), 1–4. https://doi.org/10.1029/2004GL021529.

Wakai, N., Ohyama, H., Koizumi, T., 1987. Manual of Ionogram Scaling (Third Vers). Ministry of Posts and Telecommunications, Japan, Retrieved from https://www.sws.bom.gov.au/IPSHosted/INAG/scaling/japanese_manual_v3.pdf.

Weber, E.J., Buchau, J., Eather, R.H., Mende, S.B., 1978. North-south aligned equatorial airglow depletions. J. Geophys. Res. 83 (A2), 712. https://doi.org/10.1029/JA083iA02p00712.

Wang, Ning, Guo, Lixin, Zhao, Zhenwei, Ding, Zonghua, Lin, Leke, 2018. Spread-F occurrences and relationships with foF2 and h′F at low- and mid-latitudes in China. Earth, Planets and Space 70 (1), 59. https://doi.org/10.1186/s40623-018-0821-9, In this issue.

Weber, E.J., Basu, S., Bullett, T.W., Valladares, C., Bishop, G., Groves, K., Araya, J., 1996. Equatorial plasma depletion precursor signatures and onset observed at 11° south of the magnetic equator. J. Geophys. Res. Space Phys. 101 (A12), 26829–26838. https://doi.org/10.1029/96ja00440.

Whalen, J.A., 2002. Dependence of the equatorial anomaly and of equatorial spread f on the maximum prereversal E × B drift velocity measured at solar maximum. J. Geophys. Res. Space Phys. 108 (A5), 1–9. https://doi.org/10.1029/2002JA009755.

Woodman, R.F., La Hoz, C., 1976. Radar observations of F region equatorial irregularities. J. Geophys. Res. 81 (31), 5447–5466. https://doi.org/10.1029/JA081i031p05447.